Solar FTIR measurements of NO_x vertical distributions - Part 2: Experiment-based scaling factors describing the daytime variation of stratospheric NO_x

Pinchas Nürnberg[1], Sarah A. Strode[2,3], and Ralf Sussmann[1]

[1]Karlsruhe Institute of Technology, IMK-IFU, Garmisch-Partenkirchen, Germany
[2]Goddard Earth Sciences Technology and Research (GESTAR-II), Morgan State University, Baltimore, MD, 21251 USA
[3]NASA Goddard Space Flight Center, Greenbelt, MD 20771, USA

Correspondence to: Pinchas Nürnberg (pinchas.nuernberg@kit.edu) and Ralf Sussmann (ralf.sussmann@kit.edu)

Abstract

Long-term experimental stratospheric NO_2 and NO partial columns measured by means of solar Fourier-transform infrared (FTIR) spectromertry at Zugspitze (47.42° N, 10.98° E, 2964 m a.s.l.), Germany were used to create a set of experiment-based monthly scaling factors (SF_{exp}). The underlying data set is published in a companion paper (Nürnberg et al., 2023) comprising over 25 years of measurements depicting the daytime variability of stratospheric NO_2 and NO partial columns in dependence of local solar time (LST). In analogy to recently published simulation-based scaling factors by Strode et al. (2022), we created SF_{exp} normalized to SZA = 72° for NO_2 and NO for every month of the year as a function of solar zenith angle (SZA). Apart from a boundary value problem at minimum SZA values originating in averaging over different times of the month, the obtained scaling factors $SF_{exp}(NO_2)$ and $SF_{exp}(NO)$ in dependence of SZA represent very well the daytime behavior already shown in model simulations and experiments in the literature. This behavior is a well pronounced increase of the NO_2 and NO stratospheric partial colum with the time of the day and a flattening of this increase after noon. In addition to the discussion of SF_{exp}, we validate the simulation-based scaling factors $SF_{sim}(NO_2)$ (Strode et al., 2022) and present simulation-based scaling factors for NO $SF_{sim}(NO)$. The simulation-based scaling factors show an excellent agreement with the experiment-based ones, i.e. for NO_2 and NO the mean value of the modulus between experiment and simulation over all SZA and months is only 0.02 %. We show that recently used model simulations can describe very well the real behavior of nitrogen oxide (NO_x) variability in the stratosphere. Furthermore, we conclude that ground-based FTIR measurements can be used for validation of the output of photochemistry models as well as creating experiment-based data sets describing the daytime stratospheric NO_x variability in dependence of SZA. This is a contribution to improved satellite validation and a better understanding of stratospheric photochemistry.

1 Introduction

The important role of NO_2 and NO in stratospheric photochemistry has been known for half a century (Crutzen, 1979). Both nitrogen oxides (NO_x) are a product of the photolysis of N_2O and are an important part of the ozone (O_3)-destroying nitrogen catalytic cycle which controls the O_3 abundance in the stratosphere (Johnston, 1992). Additionally, industry and transportation are major sources of tropospheric NO_x in the troposphere (Grewe et al., 2001). Especially in urban areas, it can serve as a precursor for e.g. O_3 or nitric acid (HNO_3) and therefore promote smog events and directly affect human health (World Health Organization. Regional Office for Europe, 2003). Furthermore, NO_2 has the potential to cause significant radiative forcing during pollution events with highly elevated NO_2 concentrations in the troposphere (Solomon et al., 1999).

The monitoring and quantification of NO_x total columns has been conducted since 1967 via different satellite missions (Godin-Beekmann, 2010; Rusch, 1973). For the observation of tropospheric pollution events (e.g. smog), therefore, the knowledge of the stratospheric contribution to the total column is crucial. One way to face this problem is the reference sector method, taking unpolluted total columns at a similar latitude (e.g. above the ocean) as a reference and subtract it from the total column (Richter and Burrows, 2002). The two main assumptions justifying this approach are the longitudinal homogeneity of the stratospheric column and negligible tropospheric columns over the ocean. However, due to the strong diurnal cycle of NO_2 and NO no time mismatch should occur between both columns.

One method for dealing with the problem of time and site mismatches when comparing different NO_x columns is the use of ground-based Fourier-transform infrared (FTIR) measurements. This method can provide data from any time of the day during sun light hours, giving the opportunity to describe daytime NO_x variabilities with a high precision, as done for NO_2 by Sussmann et al. (2005). For the first time, they found a reliable daytime NO_2 increasing rate of $(1.02\pm0.12)\cdot10^{14}$ cm^{-2} h^{-1} derived from FTIR measurements at mid-latitudes. Additionally, the retrieved FTIR data can have a certain altitude resolution, which allows conclusions about NO_x partial column variabilities, e.g. of the stratospheric columns (Zhou et al., 2021; Yin et al., 2019). In Part 1 of our two companion papers (Nürnberg et al., 2023) we used these advantages of ground-based FTIR measurements to retrieve stratospheric partial columns from long-term NO_2 and NO measurements above Zugspitze (47.42° N, 10.98° E, 2964 m a.s.l.), Germany, yielding information on NO_x daytime variability for every month of the year. This specific data set has the potential to improve satellite validation and can serve as a basis for the description of stratospheric NO_x variabilities with high time resolution. However, the data from ground-based measurements can only be retrieved for the limited number and locations of existing sites.

A method without this site restriction describing stratospheric NO_x concentrations with global coverage is the use of model data from three-dimensional global transport and photochemistry models. The latter are able to describe trace gas concentrations in dependence of altitude, latitude and longitude with a very good time resolution. In comparison to one-dimensional models describing only the vertical distribution of atmospheric trace gases (e.g. O_3, NO_2, NO) (Allen et al., 1984; Prather and Jaffe, 1990), three-dimensional models simulate transport fluxes in all three dimensions and are able to include nearly all feedback mechanisms of the real world (Mclinden et al., 2000; Chang and Duewer, 1979). Both types of models can account for daytime variabilities and have been used in the last decades for inter-satellite comparisons (Brohede et al., 2007; Dubé et al., 2020) as well as for satellite data validation (Bracher et al., 2005) and correction (Dubé et al., 2021; Wang et al., 2020). However, these studies differ from case to case and do not provide general global information about NO_x variability. These global information should be site independent and can be applied to any satellite validation or correction all over the planet.

Here, a recent study of Strode et al. (2022) closed this gap by developing a set of simulation-based scaling factors (SF_{sim}), which describe the daytime variability of NO_2. A given SF_{sim} is a measure for the change of trace gas concentrations during the day normalized to a specific time (here sunrise or sunset). SF_{sim} are extracted from a three-dimensional model, which considers long-range transport, stratospheric and tropospheric chemistry as well as aerosol, radiation and transport. The generated monthly output is available for latitudes between -90° and 90° (1° steps) and altitudes between 6 km and 78 km

(0.5 km steps) for every time of the day given in solar zenith angle (SZA) values (Strode et al., 2022). This extensive research opens up the opportunity for the comparison, validation, and correction of remote and ground-based data products, by overcoming time or site mismatches.

However, an observational counterpart, i.e. an analogous data set of experiment-based scaling factors describing the daytime increase of stratospheric NO_x still does not exist, due to the lack of reliable long-term data comprising the full daytime NO_2 and NO variability. To close this gap, in this paper we create a set of experiment-based scaling factors (SF_{exp}) in analogy to the simulation-based scaling factors published by Strode et al. (2002). On the one hand, this data set should serve as a general set of data describing the NO_x daytime variability in dependence of SZA for the given latitude (47° N) of our observation site. On the other hand, we would like to use it to validate the recently published model data for $SF_{sim}(NO_2)$ (Strode et al., 2022) as well as validate unpublished model data for SF_{sim}(NO) (Sarah Strode, personal communication, 2023). For this SF_{exp} data set we will use the observational results described in Part 1 of our set of two companion papers (Nürnberg et al., 2023), where a reliable long-term data set of NO_2 and NO partial columns above 16 km altitude above Zugspitze was created. As described above, these long-term data are retrieved from ground-based FTIR measurements and describe the daytime variability of stratospheric NO_x within timesteps of minutes for every month of the year. The cut-off point at 16 km was chosen to avoid influences of variabilities near the tropopause and in the boundary layer upon the stratospheric partial column. Details are discussed in part 1. It is outside the scope of this work to describe with SF_{exp} the strong and fast photochemistry at sunrise and sunset.

This paper (as Part 2 of our two companion papers) briefly describes in Sect. 2 the experimental set up and the resulting FTIR data taken from Part 1 (Nürnberg et al., 2023). In Sect. 3, the dependence on SZA for NO_2 and NO is shown and the resulting daytime variations presented in detail in Part 1 are discussed shortly, before the NO_x partial columns (> 16 km) are converted into experiment-based scaling factors ($SF_{exp}(NO_2)$ and SF_{exp}(NO)) in Sect. 4. Finally, the resulting SF_{exp} are compared qualitatively and quantitatively to SF_{sim} retrieved from model simulations.

2 FTIR data

All data of this study are retrieved from long-term ground-based FTIR solar absorption measurements at Zugspitze, Germany (47.42° N, 10.98° E, 2964 m a.s.l.). The high-altitude observatory at Zugspitze is located in the German alps and can be considered as a clean site without strong influences from pollution events in the boundary layer. The used Bruker IFS 125HR spectrometer has operated continuously since 1995 at the Zugspitze. The experimental set-up and retrieval strategy are described in our part 1 companion paper (Nürnberg et al., 2023). As described in part 1, we used daily pressure and temperature profiles from the National Centers for Environmental Prediction (NCEP) interpolated to the measurement time. The temperature dependency of the data cannot be discussed in detail here, but it is very likely that the stratospheric temperature affects the NO_x concentration and therefore also the observed diurnal cycle. The pollution filtered NO and NO_2 stratospheric partial columns (above 16 km altitude) derived in our part 1 study serve as a basis for the experiment-based scaling factors created now in this part 2) work. The data set comprises 6,213 NO and 16,023 NO_2 partial columns measured at the Zugspitze between 1995 and 2022.

3 Experimental data

3.1 NO_x stratospheric partial column dependence on SZA

Figure 1 shows the NO_2 stratospheric partial columns (black symbols) taken from Nürnberg et al. (2023) for every month as a function of SZA. Note this is the same data as shown in our Part 1 (Fig. 3 therein), which had been therein plotted as a function of local solar time. The *x*-axis is interrupted for SZA values without observations in the respective month. Here, we define

SZA to be positive in the morning from sunrise (SZA = 90°) to local solar noon (respective minimum value dependent of the season) and to be negative in the afternoon between local solar noon and sunset (SZA = -90°).

As already described and discussed in Part 1 of the two companion papers, the daytime increase of the NO_2 stratospheric partial column follows for every month a linear behavior from sunrise to sunset. Briefly, this behavior reflects the photolysis of the reservoir species HNO_3 and N_2O_5 resulting in a consecutive increase of NO_2 during daytime (Crutzen, 1970).

Figure 2 shows in a similar way the NO stratospheric partial columns (black symbols) taken from the same work for every month in dependence of SZA (Nürnberg et al., 2023). Note this is the same data as shown in our Part 1 (Fig. 5 therein) as a function of local solar time. Briefly, the data show the typical daytime increase of stratospheric NO described in the literature via model calculations (Dubé et al., 2020; Mclinden et al., 2000) or shown experimentally (Zhou et al., 2021; Rinsland et al., 1984) for every month. Here, the photolysis of the reservoir species N_2O leads to a well-pronounced increase of stratospheric NO concentration in the morning (Crutzen, 1970). After local solar noon, the shift of the NO_2-NO equilibrium, the increasing amount of O_3 and the solar elevation dependency of the involved photochemical reaction lead to a strong flattening of the daytime NO curve in dependence of SZA in comparison to NO_2. This afternoon-effect is more pronounced in the summertime (mid row) than the rest of the year (Nürnberg et al., 2023).

4 Calculation of experiment-based scaling factors

A set of experiment-based scaling factors (SF_{exp}) analogous to the model-based scaling factors (SF_{sim}) published by Strode et al. (2022) was created as follows: The mean values for 2° bins of SZA of the stratospheric partial column (> 16 km) were calculated. In a next step, these mean values were normalized to SZA = 72° resulting in monthly SF_{exp} sets for NO_2 and NO shown in Fig. 3 and Fig. 4, respectively. These data reflect the daytime variation of stratospheric NO_2 and NO above Zugspitze, Germany. Values resulting from only one measurement point are shown in red without error bar.

$SF_{\mathrm{exp}}(NO_2)$ (Figure 3, black and orange symbols) increases linearly throughout the day in each month, reflecting the increase in stratospheric NO_2 concentration. There are two observations which can be pointed out here. First, the error bars in Fig. 3 (i.e. ±2 standard errors of the mean, ±2 SEM = $\pm 2\ \sigma/\sqrt{(n)}$) are independent of the season and are very small, reflecting a low scattering within the 2° SZA bins and enough averaging data points n. Second, in spring and autumn, at local solar noon (minimum SZA), a significant increase in $SF_{\mathrm{exp}}(NO_2)$ is visible. This effect can be understood as a boundary valueproblem being due to the relatively fast change of SZA and of the NO_2 stratospheric partial column (seasonal variation) during the spring and autumn months, respectively. Here, the combination of both the SZA and stratospheric partial column changes within one month end up with an increased averaged NO_2 stratospheric partial column near the minimum SZA. The reason is that for SZA values below the minimum SZA at day 15 of each month, only partial columns from one half of the month can contribute to the average. Unfortunately, the stratospheric partial columns of this half deviate significantly from the monthly mean. Figure S1 in the supporting material illustrates this phenomenon using the NO_2 partial column above 16 km altitude. Here, the first half (red symbols) and the second half (blue symbols) of April is split up into two datasets underlining the described boundary value problem. At low SZA values, only blue data points sum up to the averaged values, considering only the second half of the month. Consequently, the partial column and of course the scaling factor increases artificially (pointed out by the blue arrow in the figure). This effect leads us to the exclusion of these data points (Figure 3, orange symbols) below the minimum SZA reached at day 15 of the respective month. Another opportunity to face this problem would be the choice of a smaller time binning (e.g. 2 weeks, 10 days). However, this would i) worsen the comparability to the simulation-based scaling factors and ii) reduce the usable data base per time bin. The whole used data set of $SF_{\mathrm{exp}}(NO_2)$ can be found in the supporting material Table S1-S4.

For $SF_{\mathrm{exp}}(NO)$ (Figure 4, black and orange symbols), the difference in daytime increase in comparison to NO_2 is very well pronounced. Before local solar noon, SF_{exp} increases for every month linearly. After local solar noon, the described flattening of the increase is visible. Here, the NO stratospheric partial column stays almost constant within the scattering until sunset independent of the season. The ±2 SEM error bars of SF_{exp}(NO) shown in Fig. 4 are also very small, but more values are excluded (red symbols) due to the availability of only one measurement point within the corresponding 2° SZA bin. This reflects the lower data base of the NO retrieval, originated in the use of another spectral micro-window for analysis. However, the small error bars underline, that for most of the mean values, the data base is reliable. Near local solar noon for SF_{exp}(NO) a similar but even less pronounced effect can be seen, as described for NO_2. Here, the deviation from the visible trend at spring or autumn months is very small. However, for consistent data handling we will also exclude the respective values (orange symbols) for SF_{exp}(NO) below the minimum SZA at each month 15^{th}. The whole used data set of SF_{exp}(NO) can be found in the supporting material Table S5-S8.

5 Model comparison of NO_x scaling factors

In the previous section, we created experiment-based averaged monthly scaling factors SF_{exp} for NO_2 and NO describing the daytime variation of stratospheric NO_x concentration above Zugspitze, Germany. Next, we will compare the discussed results for SF_{exp} to model-based scaling factors SF_{sim} for NO_2 published by Strode et al. (2022) and for NO calculated from the same GEOS-GMI model simulation as the NO_2 scaling factors. Details of the GEOS model simulation with GMI chemistry (Duncan et al., 2007; Strahan et al., 2007; Nielsen et al., 2017) are described in Strode et al. (2022) and refs therein. The model parameters and the analysis method can be found in the literature (Strode et al., 2022). The given scaling factors $SF_{sim}(NO_2)$ and SF_{sim}(NO) are available for 146 levels between 6 km and 78.5 km altitude in a 0.5 km grid and are normalized to SZA = 90° (sunrise). For a better comparison of experiment and model, we calculated mean values for SF_{sim} which also represent the stratospheric partial column above 16 km altitude. In order to do so, for each model level z, $SF_{sim}(z)$ was weighted to the mean monthly partial column profile of the given NO_x retrieval at z and SF_{sim}(> 16 km) was obtained via averaging over SF_{sim}(16 km) to SF_{sim}(78.5 km). Furthermore, SF_{sim}(> 16 km) was normalized SZA = 72° (rather than sunrise/sunset) as done for SF_{exp} in Sect. 4.

$SF_{sim}(NO_2)$ and SF_{sim}(NO) are additionally shown in Fig. 5 and Fig. 6, respectively (red line). At first appearance, SF_{exp} (black symbols) and SF_{sim} (red line) fits together very well and the model data follow the experimental daytime variation for both species NO_2 and NO.

5.1.1 Quantitative evaluation

For the quantitative evaluation of the model comparison, the residuals between experiment and model $(SF_{exp}-SF_{sim})/SF_{sim}$ are calculated for $SF(NO_2)$ and SF(NO) and are shown in Fig. 7 and Fig. 8, respectively. Additionally, the mean bias per month is shown as a mean value over all SZA (red dotted line).

The residuals of $SF(NO_2)$ (Figure 7) show over the whole year a very good agreement between experiment and model within ±0.2 %, reflecting the high quality of the GEOS GMI simulation at midlatitudes. Only for a few months, significant differences between experiment and model are visible. For April, August and September, the morning increase of NO_2 is less pronounced in the model, leading to a significant deviation from the experimental values and an underestimation of the experiment-based scaling factors SF_{exp} at noon. However, the experimental values describing the stratospheric NO_2 variability can be also influenced by tropospheric variations, because the used NO_2 partial column cannot be treated as completely independent of the tropospheric partial column (see Nürnberg et al. (2023)). Furthermore, the model data offer higher uncertainties during twilight which can lead to deviations from experiment (Alvanos and Christoudias, 2019).

Table 1 shows the mean bias (see also Figure 7, red dotted line) for every month calculated from the residuals shown in Fig. 7 together with two times the SEM ($2\ \sigma/\sqrt{(n)}$). Unfortunately, due to the small values of 2 SEM of 0.0065 % to 0.0192 % for most of the months (except March, July, October, November), 2 SEM is smaller than the mean bias. Therefore, when taking

2 SEM as a quantitative indicator, SF_{exp} and SF_{sim} agrees only in four months within the margin of error. However, when considering the mean deviation between experiment and model of below |0.068 %| per month, we can state that the model data published by Strode et al. (2022) reflect sufficiently well the experimental values retrieved from solar FTIR measurements at midlatitudes.

A very similar behavior can be obtained for SF(NO) (Figure 8). With a maximum deviation of ±0.2 % the agreement between experiment and model is very similar as seen for NO_2. However, it is remarkable, that for the months with highest SZA (January, February) the first data points after sunrise for which measurements exist (high SZA region) deviate significantly from zero. Comparing to Fig. 6, the experimental values in this region seem not to follow the continuous increase expected from model descriptions. Here, an error source of the experimental data can be the wide range in photochemical regimes along the line-of-sight of the FTIR slant column measurements at high SZA: high up in the atmosphere, the sun is already well above the horizon, so NO production has been significant already, while lower down the atmosphere is still much darker and NO levels still lower. The FTIR retrieval leads to an averaging over these effects because from the solar measurements NO slant columns along the line of sight are retrieved, and these are then converted to vertical column densities using a simple cos(SZA) airmass correction.

Furthermore, the NO increase in the morning is more pronounced in the model, leading to a significant deviation from the experimental values and an overestimation of the experiment-based scaling factors SF_{exp} at noon. In the same manner as discussed before for NO_2, the experimental values describing the stratospheric NO variability can be influenced by tropospheric variations, because the used NO partial column cannot be treated as completely independent of the tropospheric partial column (see Nürnberg et al. (2023)). Consequently, the lower stratospheric partial column in the morning is more influenced by the tropospheric partial column than in the evening.

In the same way as done for NO_2, the mean bias (see also Fig. 8, red dotted line) and 2 $\sigma/\sqrt{(n)}$ (2 SEM) are calculated and are shown in Table 2 for the NO residuals. Here, a better agreement between experiment and model can be quantified. For six months (January, June, September, October, November, December) the mean bias is smaller than 2 SEM indicating an agreement between experiment and model within the error bars. Nevertheless, this observation not only reflects a better agreement between experiment and model but can be also explained with a higher scattering of the residuals leading to a higher SEM. This can be confirmed when comparing the values for 2 SEM given in Table 1 and Table 2. With a mean 2 SEM of the residuals over all months of 0.0096 % for NO_2 and 0.0185 % for NO, respectively, the residual scattering with a similar n and a similar mean bias of 0.02 % is two times larger for NO.

In conclusion, the quantitative comparison of the experimental derived scaling factors SF_{exp} and the scaling factors derived from model simulations SF_{sim} for NO_2 and NO showed very good agreement of both data sets with a mean bias between experiment and model of only 0.02 % over all months underlining the quality of the model data at midlatitudes and the reliability of the retrieved experiment-based scaling factors.

6 Summary and Conclusions

In this work, we reanalyzed an experimental long-term data set from solar FTIR measurements over 25 years of measurement at the Zugspitze (47.42° N, 10.98° E, 2964 m a.s.l.), Germany, published in a companion paper (Part 1, Nürnberg et al., 2023). We present for the first time experiment-based scaling factors SF_{exp} in dependence of the solar zenith angle (SZA) representing monthly daytime NO_2 and NO variabilities in the stratosphere (> 16 km altitude) within timesteps of minutes. SF_{exp} is a measure for the variability of the NO_x partial column above 16 km altitude in comparison to local solar noon. We calculated SF_{exp} from the time dependent monthly NO_x partial columns (published in Part 1) by averaging over SZA bins of 2° and a normalization to the minimum SZA at day 15 of the respective month. The resulting values of $SF_{exp}(NO_2)$ and $SF_{exp}(NO)$ reflect very well the expected daytime variability of NO_2 and NO described in Part 1 (Nürnberg et al., 2023). Only the boundary values in spring and autumn months deviate significantly due to the relatively fast change of the minimum SZA during these months influencing the average value. Neglecting these values leads to two reliable experiment-based data sets for $SF_{exp}(NO_2)$ and $SF_{exp}(NO)$. Furthermore, we used these new experiment-based data sets to validate recently published simulation-based scaling factors $SF_{sim}(NO_2)$ (Strode et al., 2022) and recently calculated simulation-based scaling factors $SF_{sim}(NO)$ from a global study representing a similar latitude (47 °N). Comparing experiment and model simulation, we find an excellent agreement for stratospheric NO_2 and NO daytime variabilities with a mean bias of the modulus over all months and SZA of only 0.02 % with no significant deviating trends for boundary values. These results underline the quality of recent multi-dimensional model simulations of stratospheric trace gases, representing very well experimental data. Additionally, we showed, that ground-based FTIR measurements can provide reliable information about stratospheric NO_x variability within time steps of minutes, which can serve as a good basis for the validation of global model simulations and therefore can help to further optimize satellite validations.

The analysis method of the retrieval of stratospheric NO_2 and NO partial columns over Zugspitze, Germany, published in Part 1 of the two companion papers (Nürnberg et al., 2023) in combination with the generalization of this data by calculating unitless scaling factors *SF* and the validation of recently published model data in this paper (Part 2) can be seen as a strong tool for the further validation and correction of global model and satellite data. This approach can be taken for any ground-based FTIR spectrometer generating a global set of experiment-based stratospheric NO_2 and NO partial columns or scaling factors $SF_{exp}(NO_2)$ and $SF_{exp}(NO)$.

Data availability

The presented calculated experimental factors SF_{exp} and the used partial columns in dependent of the SZA can be found in the supporting material of this paper. The used experimental data is published along in Part 1 of the two companion papers (Nürnberg et al., 2023). Any other data of interest underlying this publication can be obtained at any time from the corresponding author on demand. The simulated scaling factors for NO2 and NO are available at this website: https://avdc.gsfc.nasa.gov/pub/data/project/GMI_SF/

Author contributions

PN optimized and performed the FTIR retrievals, made the scientific analysis, and wrote the manuscript. SAS performed the model simulations and processed the data for the comparison to experiment and supported editing of the manuscript. RS suggested this research, contributed to the design of the study, and supported editing of the manuscript.

Competing Interests

None.

Acknowledgements

Funding by the Federal Ministry of Education and Research of Germany within the ACTRIS-D project (grant no. 01LK2001B) is gratefully acknowledged. We acknowledge funding by the Helmholtz Changing Earth – Sustaining our Future research program within the Earth and Environment research field. SAS acknowledges support from NASA grant 80NSSC18K0711, the NASA Modeling, Analysis, and Prediction (MAP) Program, and computing resources from the NASA Center for Climate Simulation (NCCS) for the simulated scaling factors.

References

Allen, M., Lunine, J. I., and Yung, Y. L.: The vertical distribution of ozone in the mesosphere and lower thermosphere, Journal of Geophysical Research, 89, 4841-4872, doi: 10.1029/JD089iD03p04841, 1984.

Alvanos, M. and Christoudias, T.: Accelerating Atmospheric Chemical Kinetics for Climate Simulations, IEEE Transactions on Parallel and Distributed Systems, 30, 2396-2407, doi: 10.1109/TPDS.2019.2918798, 2019.

Bracher, A., Sinnhuber, M., Rozanov, A., and Burrows, J. P.: Using a photochemical model for the validation of NO_2 satellite measurements at different solar zenith angles, Atmospheric Chemistry and Physics, 5, 393-408, doi: 10.5194/acp-5-393-2005, 2005.

Brohede, S. M., Haley, C. S., McLinden, C. A., Sioris, C. E., Murtagh, D. P., Petelina, S. V., Llewellyn, E. J., Bazureau, A., Goutail, F., Randall, C. E., Lumpe, J. D., Taha, G., Thomasson, L. W., and Gordley, L. L.: Validation of Odin/OSIRIS stratospheric NO_2 profiles, Journal of Geophysical Research: Atmospheres, 112, doi: 10.1029/2006JD007586, 2007.

Chang, J. and Duewer, W. H.: Modeling chemical processes in the stratosphere, Annual Review of Physical Chemistry, 30, 443-469, 1979.

Crutzen, P. J.: The influence of nitrogen oxides on the atmospheric ozone content, Quarterly Journal of the Royal Meteorological Society, 96, 320-325, doi: 10.1002/qj.49709640815, 1970.

Crutzen, P. J.: The Role of NO and NO_2 in the Chemistry of the Troposphere and Stratosphere, Annual Review of Earth and Planetary Sciences, 7, 443-472, doi: 10.1146/annurev.ea.07.050179.002303, 1979.

Dubé, K., Randel, W., Bourassa, A., Zawada, D., McLinden, C., and Degenstein, D.: Trends and Variability in Stratospheric NO_x Derived From Merged SAGE II and OSIRIS Satellite Observations, Journal of Geophysical Research: Atmospheres, 125, doi: 10.1029/2019jd031798, 2020.

Dubé, K., Bourassa, A., Zawada, D., Degenstein, D., Damadeo, R., Flittner, D., and Randel, W.: Accounting for the photochemical variation in stratospheric NO_2 in the SAGE III/ISS solar occultation retrieval, Atmospheric Measurement Techniques, 14, 557-566, doi: 10.5194/amt-14-557-2021, 2021.

Duncan, B. N., Strahan, S. E., Yoshida, Y., Steenrod, S. D., and Livesey, N.: Model study of the cross-tropopause transport of biomass burning pollution, Atmospheric Chemistry and Physics, 7, 3713-3736, doi: 10.5194/acp-7-3713-2007, 2007.

Godin-Beekmann, S.: Spatial observation of the ozone layer, Comptes Rendus Geoscience, 342, 339-348, doi: 10.1016/j.crte.2009.10.012, 2010.

Grewe, V., Brunner, D., Dameris, M., Grenfell, J. L., Hein, R., Shindell, D., and Staehelin, J.: Origin and variability of upper tropospheric nitrogen oxides and ozone at northern mid-latitudes, Atmospheric Environment, 35, 3421-3433, doi: 10.1016/s1352-2310(01)00134-0, 2001.

Johnston, H. S.: Atmospheric ozone, Annu Rev Phys Chem, 43, 1-31, doi: 10.1146/annurev.pc.43.100192.000245, 1992.

McLinden, C. A., Olsen, S. C., Hannegan, B., Wild, O., Prather, M. J., and Sundet, J.: Stratospheric ozone in 3-D models: A simple chemistry and the cross-tropopause flux, Journal of Geophysical Research: Atmospheres, 105, 14653-14665, doi: 10.1029/2000jd900124, 2000.

Nielsen, J. E., Pawson, S., Molod, A., Auer, B., da Silva, A. M., Douglass, A. R., Duncan, B., Liang, Q., Manyin, M., Oman, L. D., Putman, W., Strahan, S. E., and Wargan, K.: Chemical Mechanisms and Their Applications in the Goddard Earth Observing System (GEOS) Earth System Model, J Adv Model Earth Syst, 9, 3019-3044, doi: 10.1002/2017MS001011, 2017.

Nürnberg, P., Sussmann, R., and Rettinger, M.: Solar FTIR measurements of NO_x vertical distributions: Part I) First observational evidence for a seasonal variation in the diurnal increasing rates of stratospheric NO_2 and NO, Atmos. Chem. Phys., 2023.

Prather, M. and Jaffe, A. H.: Global impact of the Antarctic ozone hole: Chemical propagation, Journal of Geophysical Research, 95, 3473-3492, doi: 10.1029/JD095iD04p03473, 1990.

Richter, A. and Burrows, J. P.: Tropospheric NO2 from GOME measurements, Advances in Space Research, 29, 1673-1683, doi: 10.1016/s0273-1177(02)00100-x, 2002.

Rinsland, C. P., Boughner, R. E., Larsen, J. C., Stokes, G. M., and Brault, J. W.: Diurnal variations of atmospheric nitric oxide: Ground-based infrared spectroscopic measurements and their interpretation with time-dependent photochemical model calculations, Journal of Geophysical Research, 89, 9613-9622, doi: 10.1029/JD089iD06p09613, 1984.

Rusch, D. W.: Satellite ultraviolet measurements of nitric oxide fluorescence with a diffusive transport model, Journal of Geophysical Research, 78, 5676-5686, doi: 10.1029/JA078i025p05676, 1973.

Solomon, S., Portmann, R. W., Sanders, R. W., Daniel, J. S., Madsen, W., Bartram, B., and Dutton, E. G.: On the role of nitrogen dioxide in the absorption of solar radiation, Journal of Geophysical Research: Atmospheres, 104, 12047-12058, doi: 10.1029/1999jd900035, 1999.

Strahan, S. E., Duncan, B. N., and Hoor, P.: Observationally derived transport diagnostics for the lowermost stratosphere and their application to the GMI chemistry and transport model, Atmospheric Chemistry and Physics, 7, 2435-2445, doi: 10.5194/acp-7-2435-2007, 2007.

Strode, S. A., Taha, G., Oman, L. D., Damadeo, R., Flittner, D., Schoeberl, M., Sioris, C. E., and Stauffer, R.: SAGE III/ISS ozone and NO_2 validation using diurnal scaling factors, Atmospheric Measurement Techniques, 15, 6145-6161, doi: 10.5194/amt-15-6145-2022, 2022.

Sussmann, R., Stremme, W., Burrows, J. P., Richter, A., Seiler, W., and Rettinger, M.: Stratospheric and tropospheric NO_2 variability on the diurnal and annual scale: a combined retrieval from ENVISAT/SCIAMACHY and solar FTIR at the Permanent Ground-Truthing Facility Zugspitze/Garmisch, Atmospheric Chemistry and Physics, 5, 2657-2677, doi: 10.5194/acp-5-2657-2005, 2005.

Wang, S., Li, K.-F., Zhu, D., Sander, S. P., Yung, Y. L., Pazmino, A., and Querel, R.: Solar 11-Year Cycle Signal in Stratospheric Nitrogen Dioxide—Similarities and Discrepancies Between Model and NDACC Observations, Solar Physics, 295, 117, doi: 10.1007/s11207-020-01685-1, 2020.

World Health Organization. Regional Office for Europe: Health aspects of air pollution with particulate matter, ozone and nitrogen dioxide : report on a WHO working group, Bonn, Germany 13-15 January 2003, Copenhagen : WHO Regional Office for Europe, https://apps.who.int/iris/handle/10665/107478, 2003.

Yin, H., Sun, Y., Liu, C., Zhang, L., Lu, X., Wang, W., Shan, C., Hu, Q., Tian, Y., Zhang, C., Su, W., Zhang, H., Palm, M., Notholt, J., and Liu, J.: FTIR time series of stratospheric NO_2 over Hefei, China, and comparisons with OMI and GEOS-Chem model data, Opt Express, 27, A1225-A1240, doi: 10.1364/OE.27.0A1225, 2019.

Zhou, M., Langerock, B., Vigouroux, C., Dils, B., Hermans, C., Kumps, N., Nan, W., Metzger, J.-M., Mahieu, E., Wang, T., Wang, P., and De Mazière, M.: Tropospheric and stratospheric NO retrieved from ground-based Fourier-transform infrared (FTIR) measurements, Atmospheric Measurement Techniques, 14, 6233-6247, doi: 10.5194/amt-14-6233-2021, 2021.

Table 1. Calculated mean bias of residuals ($[SF_{exp}-SF_{sim}]/SF_{sim}$) for every month between experiment and simulations for NO_2 and the standard error of the mean ($\sigma/\sqrt{(n)}$) of this value.

Month	**J (%)**	**F (%)**	**M (%)**	**A (%)**	**M (%)**	**J (%)**	**J (%)**	**A (%)**	**S (%)**	**O (%)**	**N (%)**	**D (%)**
mean bias	-0.0230	-0.0257	-0.0024	0.0433	0.0118	0.0683	0.0060	0.0207	0.0414	-0.0062	0.0007	-0.0204
$2\sigma/\sqrt{(n)}$	0.0132	0.0092	0.0088	0.0082	0.0065	0.0096	0.0077	0.0093	0.0081	0.0072	0.0085	0.0192
bias < 2SEM ?	No	No	Yes	No	No	No	Yes	No	No	Yes	Yes	No

Table 2. Calculated mean bias of residuals ($[SF_{exp}-SF_{sim}]/SF_{sim}$) for every month between experiment and simulations for NO and 2 times the standard error of the mean ($2\ \sigma/\sqrt{(n)}$) of this value.

Month	**J (%)**	**F (%)**	**M (%)**	**A (%)**	**M (%)**	**J (%)**	**J (%)**	**A (%)**	**S (%)**	**O (%)**	**N (%)**	**D (%)**
mean bias	-0.0045	-0.0592	-0.0220	-0.0269	-0.0714	-0.0046	-0.0889	-0.0767	-0.0068	-0.0118	-0.0096	0.0150
$2\sigma/\sqrt{(n)}$	0.0331	0.0236	0.0166	0.0110	0.0099	0.0160	0.0143	0.0102	0.0117	0.0138	0.0191	0.0425
bias < 2SEM ?	Yes	No	No	No	No	Yes	No	No	Yes	Yes	Yes	Yes

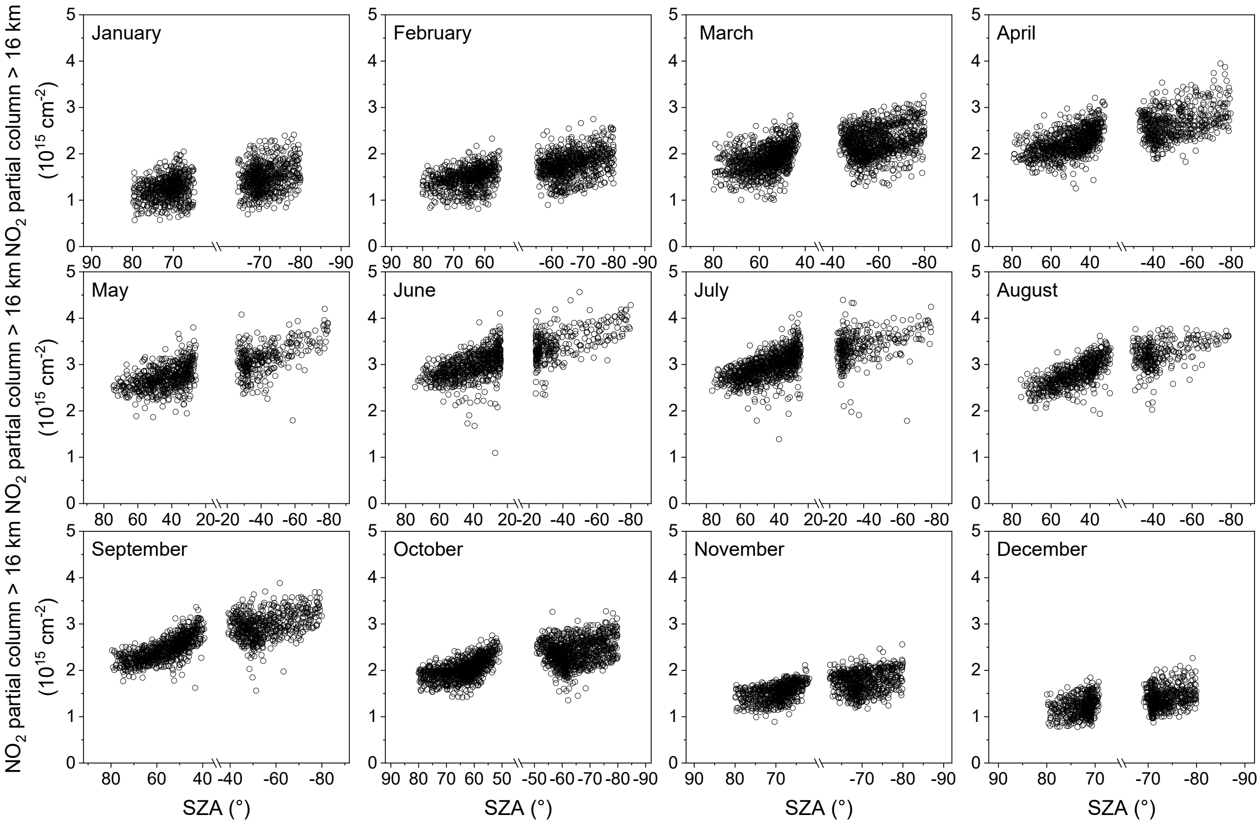

Figure 1. Retrieved NO_2 partial column above 16 km altitude measured at Zugspitze (black symbols) for every month in dependence of SZA.

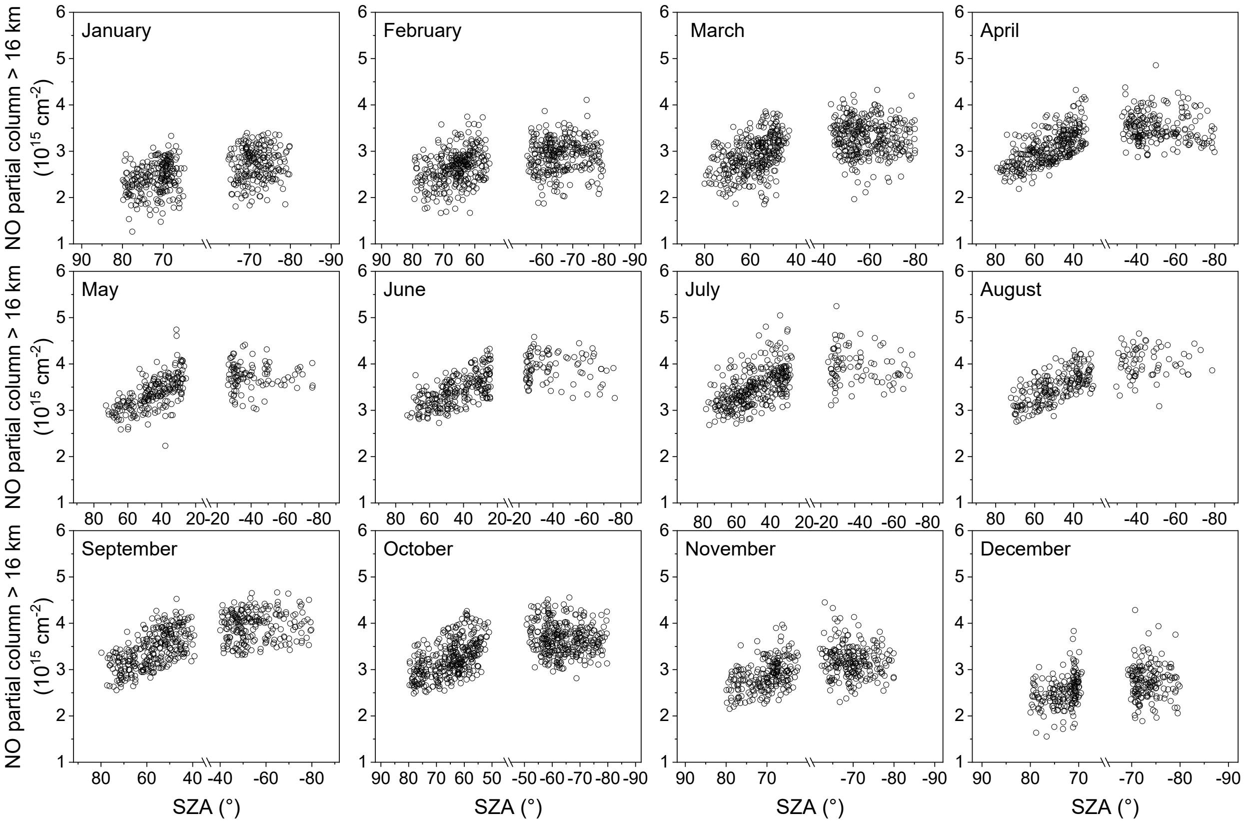

Figure 2. Retrieved NO partial column above 16 km altitude measured at Zugspitze (black symbols) for every month in dependence of SZA.

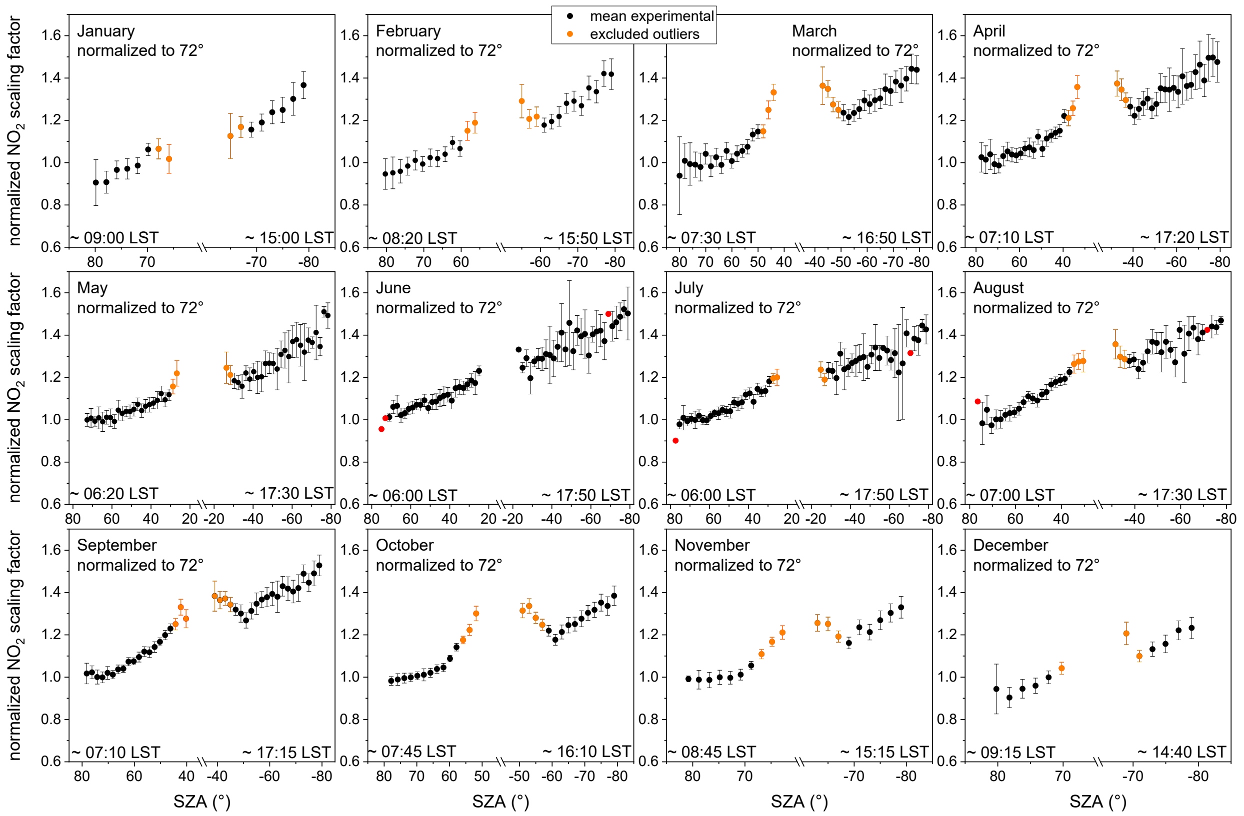

Figure 3. Calculated normalized NO_2 scaling factors $SF_{exp}(NO_2)$ above 16 km altitude measured at Zugspitze (black; orange symbols are excluded outliers) for every month in dependence of the SZA. The values represent the mean value within 2° SZA bins. The error bars represent two times the standard error of the mean ($\pm 2\ \sigma/\sqrt{(n)}$) value. Values resulting from only one measurement point are shown in red without error bar.

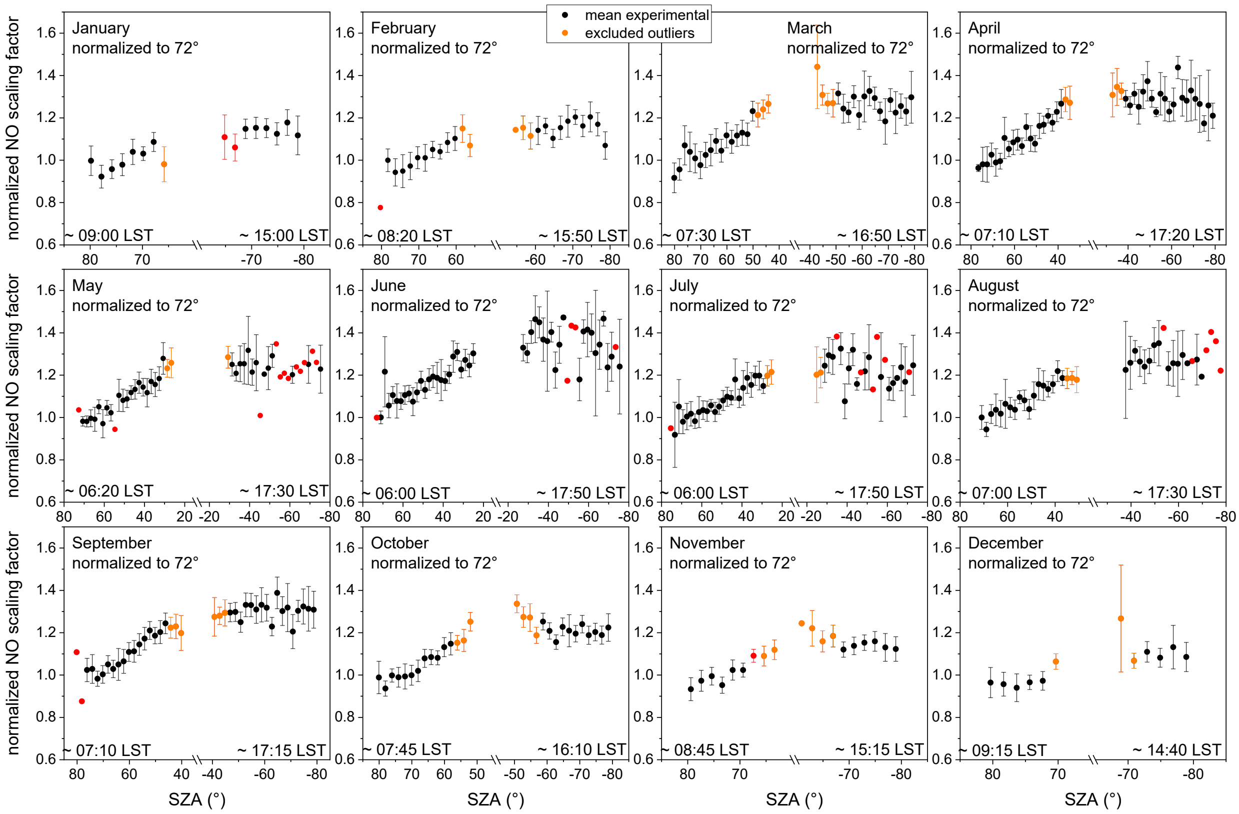

Figure 4. Calculated normalized NO scaling factors $SF_{exp}(NO)$ above 16 km altitude measured at Zugspitze (black; orange are excluded outliers) for every month in dependence of SZA. The values represent the mean value within 2° SZA bins. The error bars represent two times the standard error of the mean ($\pm 2\ \sigma/\sqrt{(n)}$) value. Values resulting from only one measurement point are shown in red without error bar.

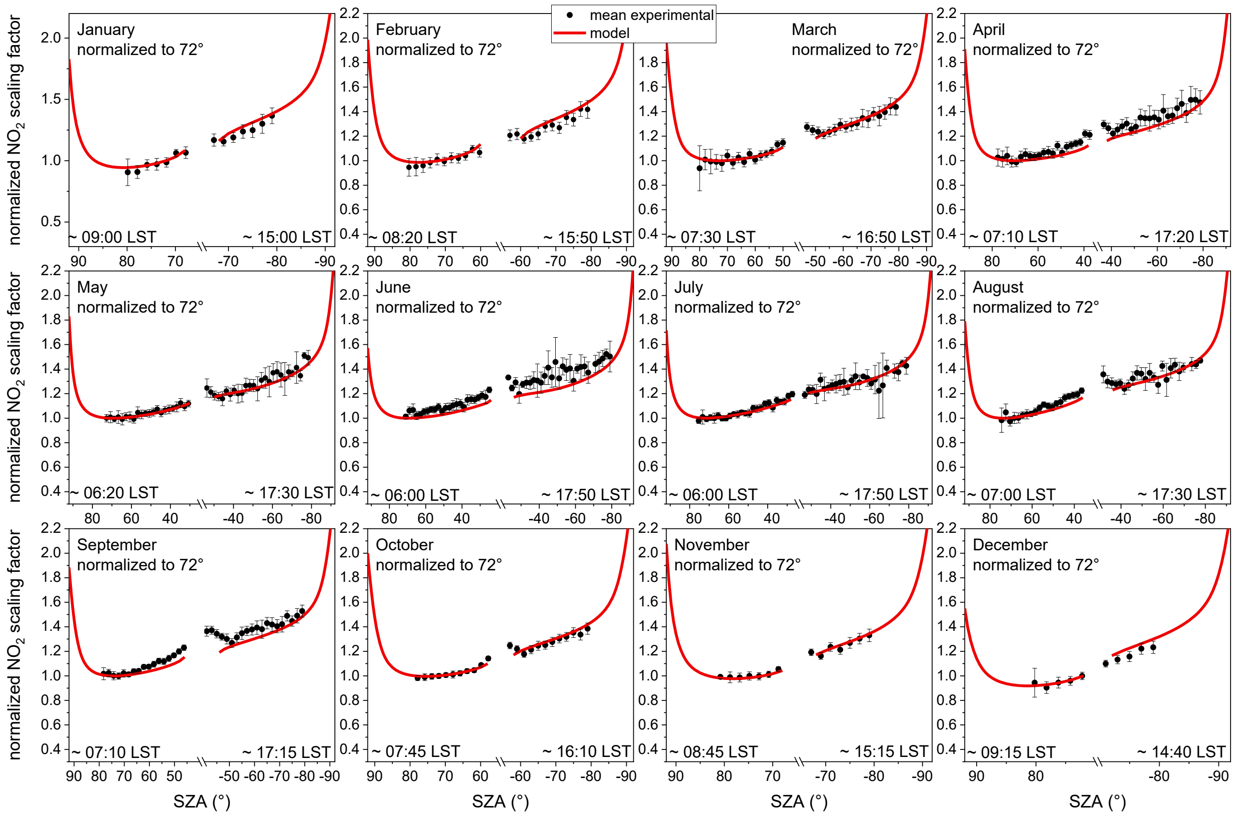

Figure 5. Calculated normalized NO_2 scaling factors $SF_{exp}(NO_2)$ above 16 km altitude measured at Zugspitze (black) and recalculated normalized NO_2 scaling factors $SF_{sim}(NO_2)$ above 16 km altitude (red line) for every month in dependence of SZA. The experimental values represent the mean value within 2° SZA bins. The error bars represent two times the standard error of the mean ($\pm 2\ \sigma/\sqrt{(n)}$) value.

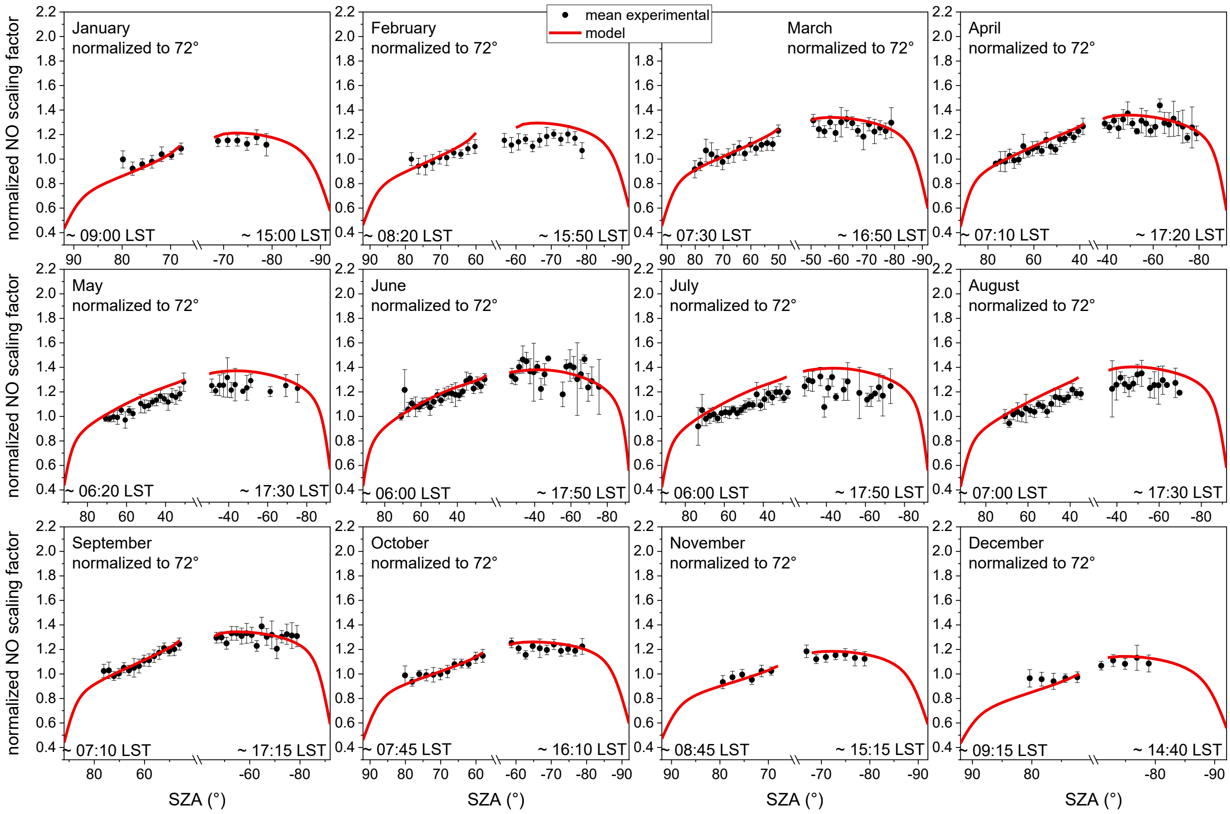

Figure 6. Calculated normalized NO scaling factors $SF_{\mathrm{exp}}(\mathrm{NO})$ above 16 km altitude measured at Zugspitze (black) and recalculated normalized NO scaling factors $SF_{\mathrm{sim}}(\mathrm{NO})$ above 16 km altitude (red line) for every month in dependence of SZA. The experimental values represent the mean value within 2° SZA bins. The error bars represent two times the standard error of the mean ($\pm 2\ \sigma/\sqrt{(n)}$) value.

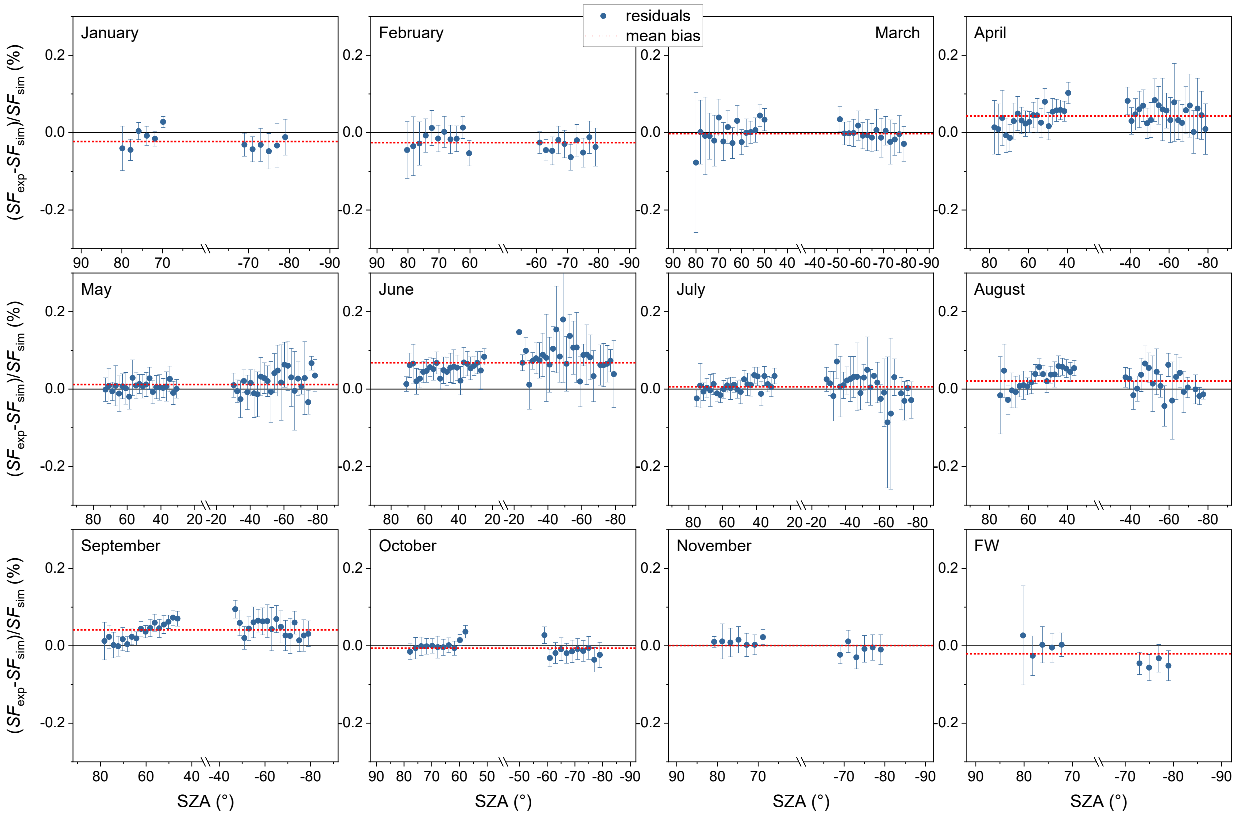

Figure 7. Calculated residuals $(SF_{exp}-SF_{sim})/SF_{sim}$ between the experimental normalized mean NO_2 scaling factors SF_{exp} and the simulated normalized NO_2 scaling factors SF_{sim} and interpoled to the respective SZA for every month in dependence of SZA. The error bars represent two times the propagated standard error of the mean ($\pm 2\ \sigma/\sqrt{(n)}$) of the experimental value. The mean bias over all SZA is shown in red.

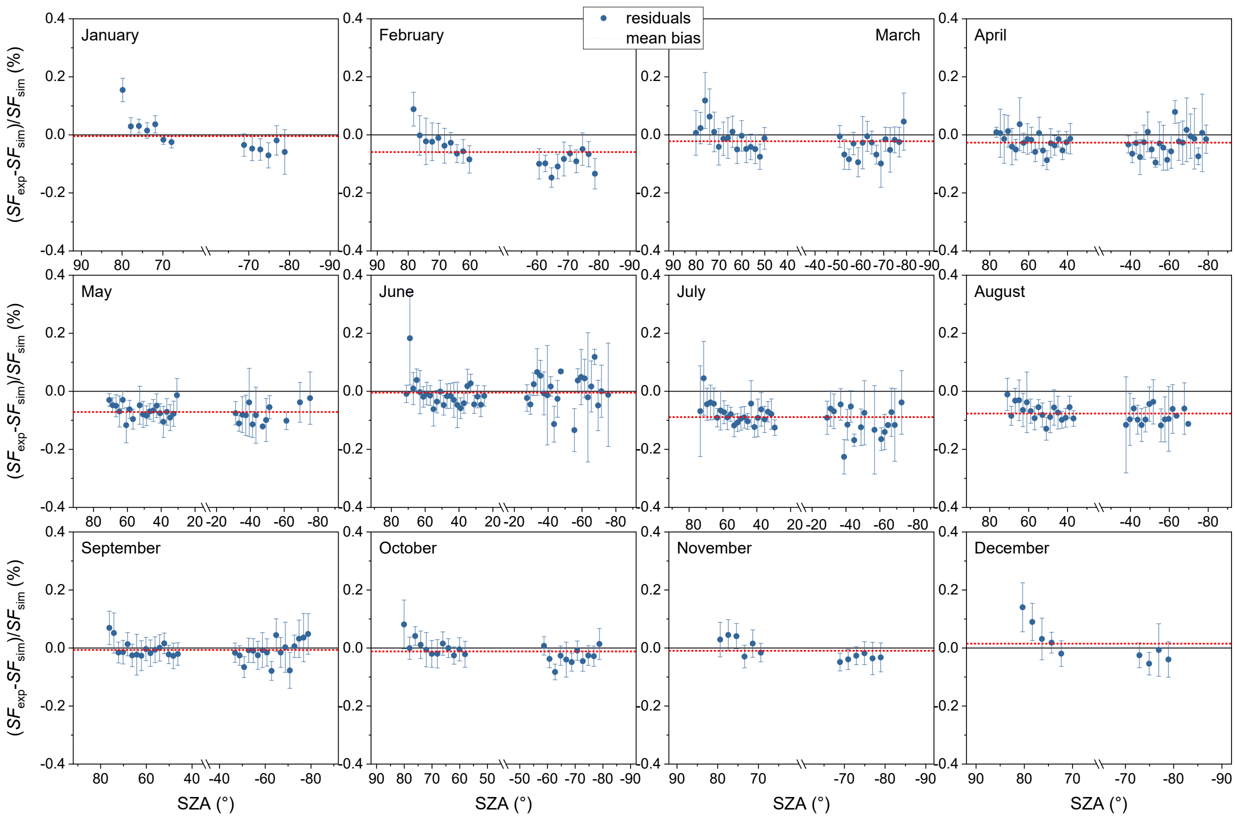

Figure 8. Calculated residuals ($[SF_{exp}$-$SF_{sim}]/SF_{sim}$) between the experimental normalized mean NO scaling factors SF_{exp} and the simulated normalized NO scaling factors SF_{sim} and interpoled to the respective SZA for every month in dependence of SZA. The error bars represent two times the propagated standard error of the mean ($\pm 2\ \sigma/\sqrt{(n)}$) of the experimental value. The mean bias over all SZA is shown in red.